European Radiology (2019) 29:3308–3316
https://doi.org/10.1007/s00330-018-5871-7

EXPERIMENTAL

Better understanding of acute gouty attack using CT perfusion in a rabbit model

Yabin Hu[1,2] · Qing Yang[1] · Yanyan Gao[3] · Xuexin Guo[4] · Yongjian Liu[5] · Can Li[6] · Yanmeng Du[7] · Lei Gao[8] · Dezheng Sun[9] · Congcong Zhu[1] · Mi Yan[1]

Received: 29 July 2018 / Revised: 16 October 2018 / Accepted: 31 October 2018 / Published online: 5 December 2018

Abstract

Objective To assess hemodynamic changes related to acute gouty knee arthritis in a rabbit with CT perfusion (CTP)

Methods Forty-two rabbits were randomly separated into two groups: the treated group of 30 and the control group of 12. The right knee was injected with monosodium urate solution and polymyxin in the treated group and saline and polymyxin in the control group. At 2, 16, 32, 48, 60, and 72 h after injection, five rabbits from the treated group and two rabbits from the control group were selected for CTP. At each time point, blood flow (BF), blood volume (BV), and clearance rate (CL) were measured, and microvessel density (MVD) was evaluated with a microscope.

Results In the treated group, BF, BV, CL, and MVD were significantly higher than in the control group ($p < 0.001$). Differences within paired comparison of BV, BF, CL, and MVD were all significant (all $p < 0.001$). Peak time of BV, BF, and MVD was 32 h and 48 h for CL. After multivariate stepwise linear regression analysis, BV was linearly associated with MVD and vice versa, which also applied to BF with MVD and BF with CL, separately. The ascending rate of MVD was the highest among that of all parameters; so was the descending rate of CL.

Conclusion CTP in this rabbit knee model accurately detected hemodynamic changes during a gouty attack.

Key Points

- *Acute gouty arthritis can be evaluated with CTP in a rabbit knee model.*
- *Following injection of MSU crystals, producing an acute gouty attack, CTP successfully assessed hemodynamic changes.*
- *The ascending rate of MVD was the highest among that of all parameters; so was the descending rate of CL.*

Keywords Perfusion imaging · Multidetector computed tomography · Arthritis, gouty · Rabbits

Abbreviations

3D	Three dimensional
BF	Blood flow
BV	Blood volume
CL	Clearance rate
CTP	Computed tomography perfusion
ICC	Intraclass correlation coefficient
MSU	Monosodium urate
MVD	Microvessel density

✉ Qing Yang
yangqingqdfy@126.com

[1] Department of Radiology, Affiliated Hospital (Laoshan Hospital) of Qingdao University, Qingdao 266000, Shandong, China

[2] Department of Radiology, Zhongshan Hospital, Fudan University, Shanghai Institute of Medical Imaging, Shanghai, China

[3] Department of Endocrinology, Affiliated Hospital (Laoshan Hospital) of Qingdao University, Qingdao, Shandong, China

[4] Department of Radiology, Dongying People's Hospital, Dongying, Shandong, China

[5] Department of Radiology, Hiser Medical Center of Qingdao, Qingdao, Shandong, China

[6] Department of CT, Juancheng People's Hospital, Juancheng, Heze, Shandong, China

[7] CT scan Room, Jinan Fourth Hospital, Jinan, Shandong, China

[8] Department of CT, The Third Hospital of Hebei Medical University, Shijiazhuang, Hebei, China

[9] Department of Radiology, Qingdao Municipal Hospital, Qingdao, Shandong, China

Introduction

Gout is an intense inflammatory reaction triggered by the deposition of monosodium urate (MSU) in joints. The prevalence of gout and hyperuricemia has increased rapidly over the recent years [1]. A variety of researches about the pathophysiology of a gout attack have been reported, focusing on inflammatory cells, immunoglobulin, and cytokines; however, they did not address vascular/hemodynamic changes that play a central role in the acute inflammatory process [2]. Acting like foreign bodies, MSU crystal deposits in joints trigger the host defense. Arteriolar dilation and angiogenesis are activated to support the host defense, inducing hemodynamic changes in the area of the involved joint [3, 4]. Blood flow (BF), blood volume (BV), and permeability are important parameters [5] and can be evaluated with CT perfusion (CTP). Therefore, the idea was that CTP might be useful to depict hemodynamic changes associated with an acute gout attack.

CTP has been widely used in many organs [5], though rarely applied in the study of the musculoskeletal system, in part because of its wide anatomical range. With the development of machines with 16 cm coverage, it is easier to examine a whole human joint in one single rotation without table movement, which is an advantage over 64- or 128-row machines with a smaller coverage [6, 7] and provides a more reliable access to hemodynamic parameters [8].

The mechanism of acute gouty arthritis is complicated, and still many features including vascular reaction need to be explored. The radiation dose of CTP is usually higher than the standard clinical dose [6], and the tophi sample is difficult to obtain owing to the unwillingness of patients to undergo invasive biopsy; therefore, animals are more appropriate than humans for CTP scanning.

Our purpose in this study was to investigate the hemodynamic changes of acute gouty arthritis in knees of rabbits by dynamic volume CT perfusion and discuss the effects of the vascular reaction during the gout attack.

Materials and methods

Animals

We chose the knees of rabbits for CTP because they can be measured more efficiently and accurately on images than those of mice due to the larger size. From September 2017 to March 2018, a total of 42 healthy male white New Zealand rabbits, 60 weeks old and weighing 2.5 ± 0.5 kg, were provided by the breeding center of Xiling in Jinan with animal certificate number SCXK (Lu) 20100005. The rabbits were acclimatized to the treated animal center of The Affiliated Hospital of Qingdao University for 1 week before the study; in addition, they were housed with standard diet and circadian rhythm synchronized with a 12-h:12-h light–dark cycle. The animal ethics committee of The Affiliated Hospital of Qingdao University approved this protocol.

Preparation of MSU crystals

MSU crystals were prepared under pyrogen-free conditions using previously described methods [7].Briefly, 4 g uric acid was dissolved in 800 ml deionized water, heated to 60 °C, adjusted to pH 8.9 with 0.5 N NaOH, and allowed to crystallize overnight under room temperature. MSU crystals were recovered by centrifugation, washed with distilled water, and dried at 40 °C for 24 h. Crystal birefringence and shape were evaluated through compensated polarized light microscopy. MSU crystals were milled and then disinfected by heating at 180 °C for about 2 h before each procedure. Less than 0.015 EU/ml endotoxin was assessed during MSU crystal preparations by *Limulus* amebocyte lysate assay (E-Toxate Kit, Sigma-Aldrich S.R.L.).

Rabbit model and study design

Forty-two rabbits were randomly allocated by a random number table to the treated group (30 rabbits) and control group (12 rabbits). In the treated group, the unbroken skin of the right knee was disinfected by alcohol, and then the knee was gently bent for the injection into the articular cavity from the lateral knee with 0.4 ml MSU solution of a mass concentration of 50 mg/ml and polymyxin; then, the knee was moved manually with the flexion–extension movement for 5 min. The right knee of the control group was treated as previously described except for the replacement of MSU solution with saline solution. If the interval time between the creation of an animal model and the CT scan was more than 8 h, the rabbits would not be fed routinely until the end of the model (Fig. 1).

CT perfusion performance

The baseline CT was performed 2 h after injection because of the necessary delay for CT preparation. The intravenous injection catheter, through which each animal was sedated with 3% pentobarbital sodium solution before CT scan, was placed in the auricular vein of a rabbit. At 2, 16, 32, 48, 60, and 72 h after injection of the MSU solution, five rabbits from the treated group and two rabbits from the control group were picked for CT scanning in each time point. The rabbit was localized supine on a Lucite board to assist accurate positioning and avoid catheter motion during transport to the scanner. The rabbit was transported to CT (Aquilion ONE; Canon Medical Systems) and placed in the same position. The scan parameters were 100 kV tube voltage, 90 mA tube current, 0.5 mm slice thickness, 512 × 512 matrices, 320 mm field of view (FOV), 0.5 s rotation time, and 0.5 mm × 320 collimator.

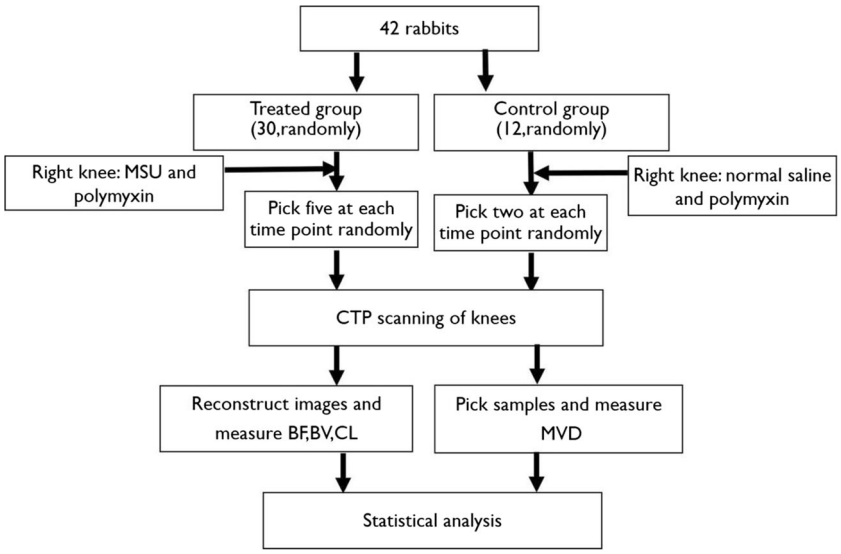

Fig. 1 Flow diagram of the experiment process

The whole knee and hypogastric region of each rabbit were covered by a single scan without bed displacement. The first images were acquired before the injection to obtain baseline images. Then, a total of 3 ml of iohexol (350 mg/ml, GE Healthcare) was administered at a flow rate of 0.8 ml/s using a dual-shot injector through the intravenous injection catheter. Three milliliters of 0.9% saline chaser was followed by the same flow speed after the injection of iohexol. CTP started after the injection, and a volume of CTP images was acquired every 2-s interval from 1 to 30 s and then 3-s interval from 31 to 90 s. Reconstructed images had a voxel size of 0.47 × 0.47 × 0.5 mm.

CTP measurements

All CTP images were transferred to an image-processing workstation (Vitrea fX, v6.0; Vital Images). Regions of interest (ROI) were placed on the abdominal aorta to generate inflow time–density curves. Subsequently, pseudo-color functional maps of transverse and 3D images were generated automatically including BF (ml/min/100 ml), BV (ml/100 ml), and clearance rate (CL, ml/min/100 ml) maps. All CTP images were independently reviewed by two musculoskeletal radiologists with 5 and 8 years of experience, who were blinded to the group, time points, and MVD. Three ROIs, a circle of 2 mm diameter each, were depicted. The average value of six ROIs in one knee put by two radiologists was recorded as the final value of CTP parameters. It is noteworthy that CL represented the permeability of microvasculature, which is similar to the permeability–surface area product (PS).

Histological assessment

Synovial tissues, which were around the intercondylar fossa of the femur from the rabbit knees, were isolated at 2, 16, 32, 48, 60, and 72 h after injection of the MSU solution, fixed in 10% neutral formalin, and embedded in paraffin. Then, the rabbit was euthanized by pentobarbital overdose. The synovial tissue slides were stained with hematoxylin and eosin. Immunohistochemical staining of CD34 was performed to quantify microvessel density (MVD), which was counted by a musculoskeletal pathologist under 100 magnification of a light microscope (Nikon Ti), focusing on microscopic fields with intense distributions of capillaries and small venules. The average counts of the five highest microscopic fields were recorded as MVD.

The pathologist (7 years of experience) was blinded to the group, CTP imaging data, and time points.

The rate of CTP parameters and MVD

The rate indicated the rising or falling speed of the parameters and MVD over time. The rate of BV, BF, CL, and MVD was calculated as follows:

$$\text{Ascending rate} = (\text{maximum value of 2 h})/(\text{value of 2 h} \times \text{hours of ascending period})$$

$$\text{Descending rate} = (\text{maximum value of 72 h})/(\text{maximum} \times \text{hours of descending period})$$

Statistical analysis

Data were expressed as mean ± standard error with normal distribution or median (25th percentile, 75th percentile) with abnormal distribution. Shapiro–Wilk tests were performed to test the normality of the distributions of the variables. Statistical significance between two groups was calculated with the Mann–Whitney U test or Student's t test according

to the distribution of variables. One-way ANOVA was performed for the comparisons among more than two groups. The post-test (Games–Hotwell's or Tukey multiple comparison test) in ANOVA was determined by Levene's test. Pearson or Spearman rank correlation analysis was used to assess the correlations among BV, BF, CL, and MVD depending on the distribution of variables. The multivariate stepwise linear regression analysis was also performed for the perfusion parameters and MVD. Interobserver agreement was evaluated by reliability analysis. Intraclass correlation coefficient (ICC) values of less than 0.40 indicated slight agreement; values of 0.40–0.75, fair agreement; and values greater than 0.75, substantial agreement. Tests were always two sided, and $p < 0.05$ was considered significant. Every analysis was performed using Statistical Package for the Social Sciences software (version 22.0, IBM SPSS Inc.).

Results

The CTP rabbit model with acute gouty arthritis of the knees was created successfully. Figure 2a–e shows the 3D and transverse pseudo-color functional maps of BV, BF, and CL from the knees of the rabbit model in the treated group. The neovascularization of synovial membrane on the rabbit knees could be seen clearly in Fig. 2f.

The values and curves of CTP findings and MVD

The values of BV, BF, CL, and MVD in the treated group were significantly higher than those of the control group (all $p < 0.001$) (Table 1). The values of CTP parameters and MVD of the treated group and the control group at each time point are summarized in Table 2. The correlations of paired comparisons among BV, BF, CL, and MVD from the treated group were all significant (all $p < 0.001$) (Fig. 3). From the time–parameter value curves, BV, BF, and MVD of the treated group had the similar shape of curves which had ascending trends at the interval between 2 and 32 h and descending trends at the interval between 32 and 72 h. However, the curve of CL of the treated group had an ascending trend at the interval between 2 and 48 h and descending trends at the interval between 48 and 72 h. The peak of the CL curve was later than those of BF, BV, and MVD for 16 h in the treated group (Fig. 4).

Regression analysis among CTP parameters and MVD

After multivariate stepwise linear regression analysis, the regression models included BV and BF when MVD was used as the dependent variable, MVD when BV is the dependent variable, CL and MVD when BF is the dependent variable, and BF when CL is the dependent variable, separately (Table 3). Interestingly, we found that BV was linearly associated with MVD and vice versa, while the other parameters were

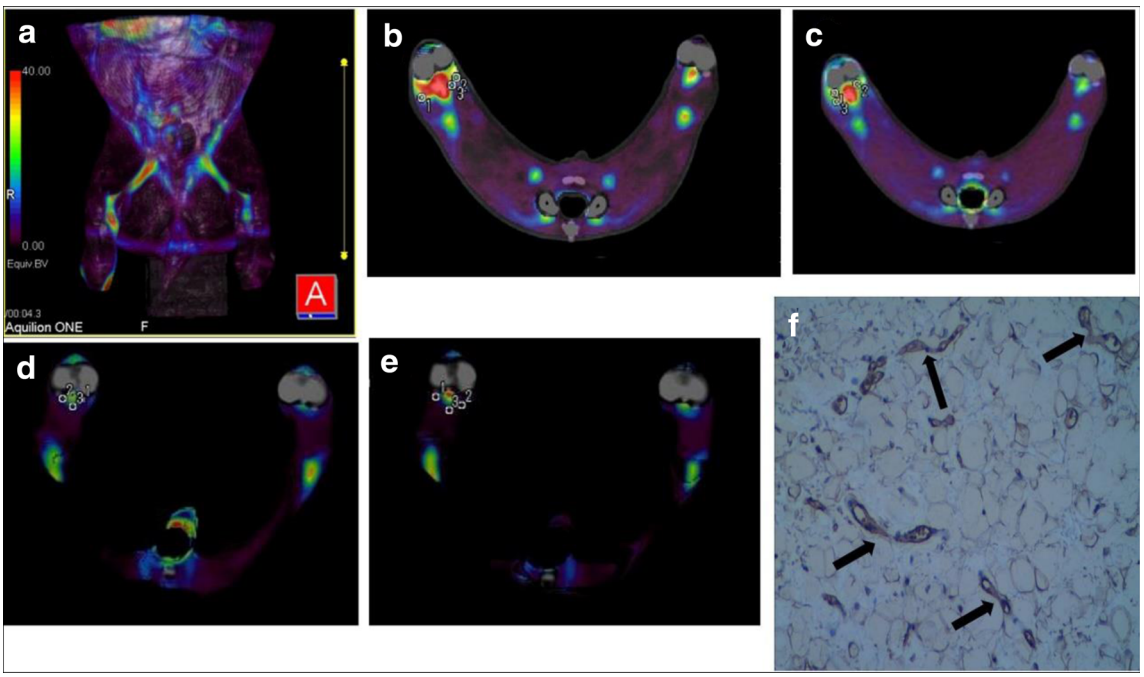

Fig. 2 **a**–**d** All belong to the treated group. 3D pseudo-color functional maps of BV at 32 h. Transverse pseudo-color functional maps of BV (**b**), BF (**c**), and CL (**d**) at 32 h. **e** The transverse pseudo-color functional maps of BV at 32 h in the control group. **f** The pathological picture of the right knee at 32 h in the treated group shows neovascularization (black arrow) under a magnification of × 100 of a light microscope

Table 1 The CTP parameters and MVD of the treated group and the control group

	BV (ml/100 ml)*	BF (ml/min/100 ml)†	CL (ml/min/100 ml)*	MVD*
Treated group ($N = 30$)	15.45 ± 0.88	188.65 (143.25, 250.9)	8.39 ± 0.46	8.77 ± 0.66
Control group ($N = 12$)	4.94 ± 0.7	38.44 ± 3.64	3.78 ± 0.65	0
t or Z	$t = 9.32$	$Z = -5.012$	$t = 5.54$	–
p	< 0.001	< 0.001	< 0.001	< 0.001

CTP CT perfusion, *BV* blood volume, *BF* blood flow, *CL* clearance rate, *MVD* microvessel density

* Data are the mean ± standard error, calculated using Student's t test (t value)

† Data are median (25th percentile, 75th percentile), calculated using Mann–Whitney U test (Z value)

controlled in the regression analyses, which also applied to BF with MVD, BF, with CL, separately. However, there was no linear relationship between BV and BF, CL, and MVD, separately (Fig. 5).

The value of rate in CTP parameters and MVD

Because of the different peak time of the parameter curves, we showed more specific rate formulas of parameters as follows:

ascending rate = (value of 32 h - value of 2 h)/(value of 2 h × 30 h)

and descending rate = (value of 32 h - value of 72 h)/(value of 32 h × 40 h) for BV, BF, and MVD,

ascending rate = (value of 48 h - value of 2 h)/(value of 2 h × 46 h) and descending rate = (value of 48 h - value of 72 h)/(value of 48 h × 24 h) for CL, separately (Table 4).

With Levene's test being significant ($p < 0.001$), the ascending rates were analyzed using one-way ANOVA ($F = 40.46$, $p < 0.001$) followed by Games–Hotwell's multiple comparison test; as a result, there were significant differences between MVD and BV, MVD and BF, and MVD and CL, separately (all $p < 0.05$). Because Levene's test was not significant ($p = 0.085$), descending rates were tested by one-way ANOVA ($F = 128.7$, $p < 0.001$) followed by Tukey post-test adjustment; then, the comparisons between CL and BV, CL and BF, and CL and MVD were all significant, separately (all $p < 0.001$).

The ascending rate of the MVD curve is higher than those of BV, BF, and CL, which indicated the rising speed of MVD is the fastest. The descending rate of the CL curve is higher than those of BV, BF, and MVD, which suggested the falling speed of CL is the fastest (Fig. 6).

Interobserver agreement in CTP parameters

The two observers in our study showed substantial interobserver agreement for measurement of the BV (ICC = 0.842), BF (ICC = 0.878), and CL (ICC = 0.862).

Table 2 The CTP parameters and MVD of the treated group in each time point

Time point (h)		N	BV (ml/100 ml)	BF (ml/min/100 ml)	CL (ml/min/100 ml)	MVD	p value
2*	Treated group	5	8 ± 0.12	131.62 ± 1.24	5.34 ± 0.2	3.4 ± 0.24	< 0.001
	Control group	2	4.6	33	3.01	0	
16*	Treated group	5	11.7 ± 0.41	176.36 ± 2.01	7.26 ± 0.33	6.4 ± 0.24	< 0.001
	Control group	2	4.9	39.9	4.55	0	
32*	Treated group	5	22.18 ± 0.4	259.48 ± 0.79	8.68 ± 0.22	13.6 ± 0.4	< 0.001
	Control group	2	5.1	42.75	5.45	0	
48*	Treated group	5	19.32 ± 0.53	250.84 ± 1.45	12.48 ± 0.17	12.4 ± 0.24	< 0.001
	Control group	2	5.5	46.7	3.9	0	
60*	Treated group	5	16.8 ± 0.17	196.72 ± 0.39	10.26 ± 0.2	9.2 ± 0.37	< 0.001
	Control group	2	5.3	39.9	4.21	0	
72*	Treated group	5	14.72 ± 0.25	143.72 ± 1.41	6.32 ± 0.16	7.6 ± 0.4	< 0.001
	Control group	2	4.7	35.6	3.5	0	

Data of the treated group are expressed as mean ± standard error, calculated using one-way ANOVA followed by Bonferroni's multiple comparison test at every time point. Data of the control group are expressed as mean and have no statistical treatment because its number is too small. P values were calculated with the one-way ANOVA and showed the difference among BV, BF, CL, and MVD of the treated group in every time point

CTP CT perfusion, *BV* blood volume, *BF* blood flow, *CL* clearance rate, *MVD* microvessel density

* All $p < 0.008$ in Bonferroni's multiple comparison test

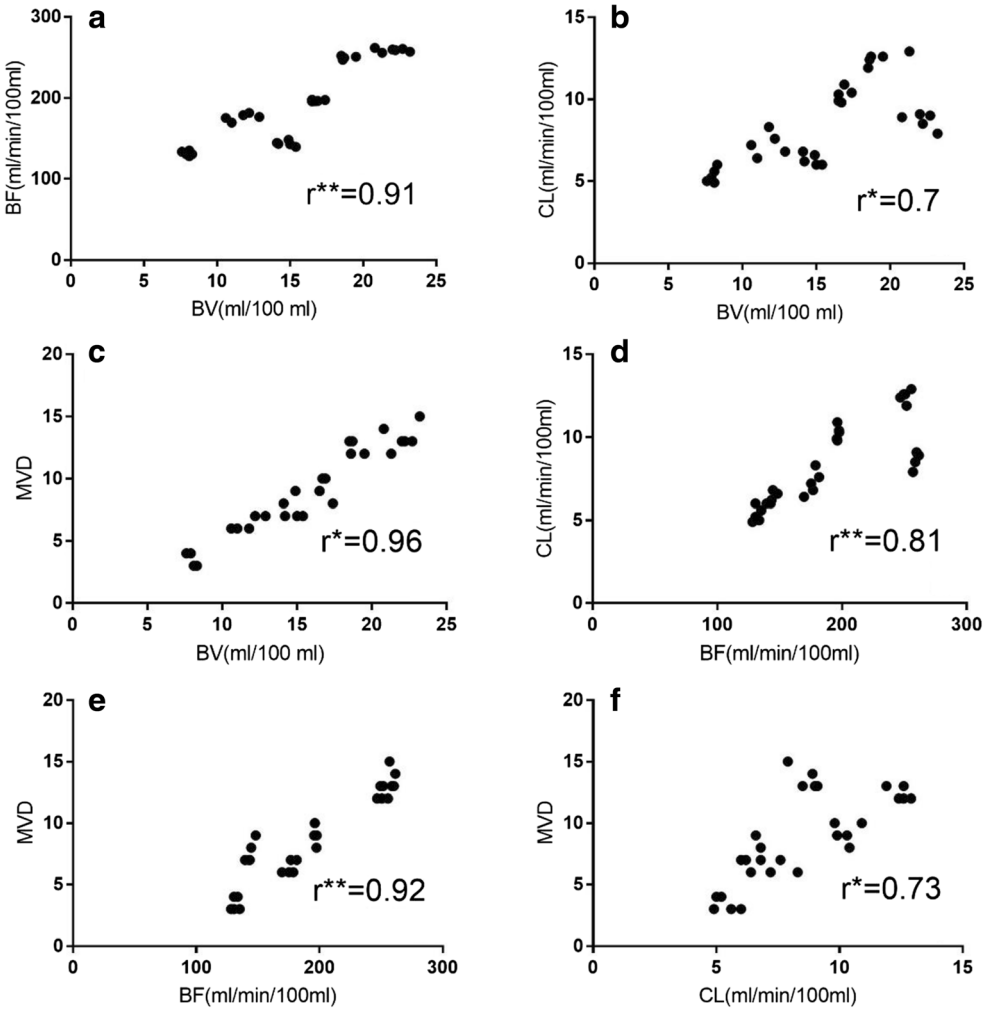

Fig. 3 The scatterplots of the paired comparisons among BV, BF, CL, and MVD. **b**, **c**, and **f** Asterisk indicates Spearman correlation analysis for comparison. **a**, **d**, and **e** Two asterisks indicate Pearson correlation analysis for comparison. *r*, correlation coefficient. The correlations of paired comparisons among BV, BF, CL, and MVD were all significant (all $p < 0.001$)

Discussion

The present study shows that acute gouty arthritis could be evaluated with CTP in a rabbit knee model according to hemodynamic changes. Additionally, the ascending rate of MVD was the highest among those of all the parameters; so was the descending rate of CL.

A variety of animal models have been used to investigate the acute inflammation in gouty arthritis in previous researches. Phelps and McCarty reproduced an acute gouty episode by injecting 20 mg of MSU crystals into a canine animal model [8]. Subsequently, murine models of ankles by injecting MSU crystals have been utilized to study the pathogenesis of acute gouty arthritis [9]. The role of locally produced IL-8, in knee joints injected with MSU crystals, was evaluated in an adult Japanese female rabbit model [10].

Ultrasound has been employed to assess the inflammatory and structural joint changes in the knees of a rabbit model of gout attack [11]. As far as we know, there are no animal models that reported the use of CTP guidance to assess the hemodynamics of acute gouty arthritis in the knees of a rabbit model. CT perfusion was used in our study because it is a noninvasive imaging modality that enables repeated quantification of various parameters of tissue perfusion [12]. The volume CT expands traditional regional CT perfusion to whole-organ CT perfusion, thereby providing comprehensive perfusion information. With a maximum detector width of 16 cm, it enables the entire knees and abdominal aorta of rabbits to be examined in a single rotation and create an image with isotropy of time. Furthermore, a large cone angle may lead to a smaller contribution of overbeaming to the total radiation dose.

At the interval between 0 and 32 h, BV, BF, and MVD all increased, but CL rose at the interval between 0 and 48 h. With intra-articular depositions of MSU crystals through injection, neutrophils are recruited to ingress into the joint cavity, where they can be activated by direct contact with crystals and then be removed by differentiation of infiltrating monocytes into macrophages [3].

A variety of neutrophils are needed to support the host defense as described. Arteriolar vasodilation occurs, leading to increased blood flow and engorgement of the downstream

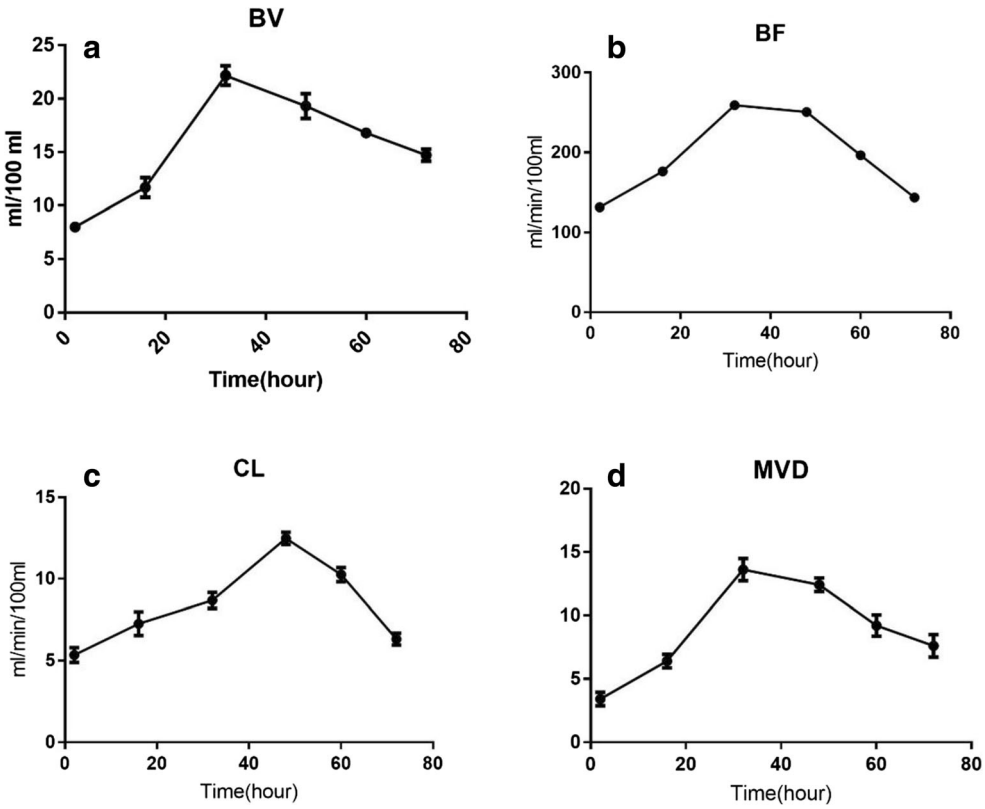

Fig. 4 The curves of parameters over time. BV (**b**), BF (**c**), and MVD (**d**) had a similar shape of curves, but the peak of the CL curve was later than those of BF, BV and MVD for an interval of 16 h. BV, blood volume; BF, blood flow; CL, clearance rate; MVD, microvessel density

capillary beds, locally. New capillary networks also form by angiogenesis and result in the expansion of the microvasculature, leading to an increase in the blood flow and blood volume. Meanwhile, the microvasculature becomes much permeable because of structural abnormalities in neovascularization [4]. Nevertheless, MVD is not linearly associated with CL, which indicates that angiogenesis is not a primary factor affecting the increased CL. Histamine, kinins, and other mediators may play crucial roles in increasing vascular permeability which helps neutrophils to exudate into the joint cavity. The rising speed of MVD is faster than that of BV, BF, and CL. Vessels are the structural basis of perfusion parameters, so the angiogenesis must develop very early to support the increasing BV, BF, and CL.

Acute gout is an auto-inflammatory disease characterized by self-limiting inflammation even without treatment, in the joints or tissues with the deposition of MSU crystals [13]. In our study, descending trends of BV, BF, and MVD started at 32 h, and CL at 48 h, in rabbit knees, which support the character of spontaneous resolution of the gout attack. Recent researches have now shown that phagocytosis of apoptotic neutrophils by neutrophils contributes to the resolution

Table 3 Multivariate stepwise linear regression analysis of the CTP parameters and MVD of the treated group ($N = 30$)

Dependent variable	Independent variables	Included variables	coefficients	Standard error	Standardized coefficients	*p* value
MVD	BV, BF, CL					
		BV	0.484	0.07	0.649	< 0.001
		BF	0.025	0.007	0.352	= 0.001
BV	BF, CL, MVD					
		MVD	1.289	0.07	0.961	<0.001
BF	BV, CL, MVD					
		MVD	10.246	1.285	0.743	< 0.001
		CL	5.027	1.848	0.253	= 0.011
CL	BV, BF, MVD					
		BF	0.04	0.006	0.798	< 0.001

CTP CT perfusion, *BV* blood volume, *BF* blood flow, *CL* clearance rate, *MVD* microvessel density

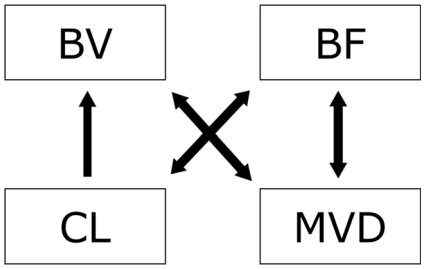

Fig. 5 The relationships among BV, BF, CL, and MVD through multivariate stepwise linear regression analysis. BV was linearly associated with MVD and vice versa, while the other parameters were controlled in the regression analyses, which also applied to BF with MVD and BF with CL, separately. However, there was no linear relationship between BV and BF and CL and MVD, separately

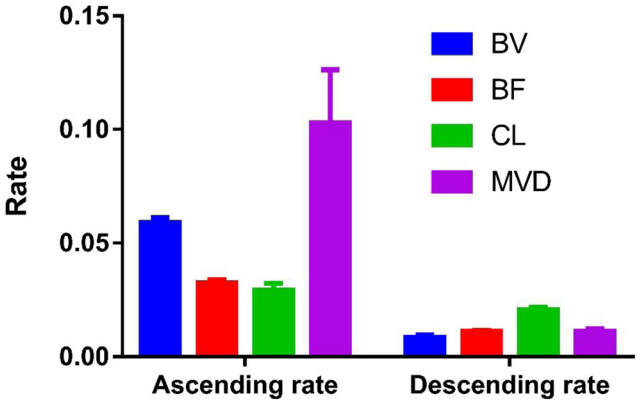

Fig. 6 The rates of BV, BF, CL, and MVD in ascending and descending trends. The ascending rate of the MVD curve is larger than those of BV, BF, and CL, and the descending rate of the CL curve is higher than all the other parameters

of the gout attack. Induction of TGFβ1 production through apoptotic cell clearance may play a crucial role in controlling gouty inflammation by limiting both pro-inflammatory functions and inflammatory cell infiltration. TGFβ1 reinforces shutdown of inflammatory cell functions in both neutrophils and macrophages, including inhibition of amplification of IL-1β signaling [14]. IL-1β is widely considered as an essential factor to the initiation of the inflammatory cascade that culminates in a gouty attack [15]. The generation and release of neutrophil extracellular traps (NETs) by activated neutrophils is an efficient defense system according to the function of neutrophils trapping and killing pathogens [16]. Distinct from necrotic cell death and neutrophil apoptosis, non-inflammatory NETs provide a different mechanism of efficient shutdown and removal of neutrophils, thereby supporting resolution of inflammation [16].

The peak of the CL curve was later than those of BF, BV, and MVD for 16 h. More leukocytes, emigrating from the vessel wall by a rising permeability of vessels, prepare for the spontaneous resolution of inflammation, because they can provide neutrophils phagocytosing apoptotic neutrophils, apoptotic cell clearance inducing TGFβ1, and activated neutrophil-generating NETs.

The descending rate of the CL curve is higher than that of BV, BF, and MVD. Normalization of vascular permeability can slow down the movement of fluid containing leukocytes, chemical mediators, and water from capillaries into the extravascular tissues. Therefore, the reduction of CL is a crucial element to the resolution of inflammation. With the resolution of inflammation, there is no need for the transportation of inflammatory cells and cytokines, leading to the reduction of BV and BF. Subsequently, regression of angiogenic capillaries occurs, which may be due to the reduction of BV and BF, because there is a linear relationship between BV and MVD and BF and MVD, separately. Eventually, the combined efforts of lymphatic drainage and macrophage ingestion of necrotic debris lead to the clearance of inflammatory cells and detritus from the battlefield [17].

There are several limitations in this research. First of all, the sample size was relatively small which may result in potential bias. Secondly, our software only permitted ROIs drawn in a single image plane and made it impossible to use volumes of interest for the analysis of perfusion parameters, which would have represented a more robust approach. Thirdly, the gout attack model which responded with a local inflammatory reaction by injecting exogenous synthetic MSU crystals was different from the local inflammatory process triggered by endogenous MSU crystals in the synovial membrane. Last but not the least, 72 h might be too short for evaluating intra-articular changes due to MSU–crystal injections, so it would be proper to monitor the intra-articular changes for a longer period.

In conclusion, this rabbit knee model by injection of MSU crystals effectively performed an acute joint inflammatory

Table 4 Rate of the CTP parameters and MVD of the treated group ($N = 30$)

	BV	BF	CL	MVD	Levene's test	ANOVA	Post-test
Ascending rate*	0.0591 ± 0.0009	0.0324 ± 0.0007	0.0293 ± 0.0014	0.1028 ± 0.0105	$p < 0.001$	$p < 0.001$	Games–Hotwell
Descending rate†	0.0084 ± 0.0005	0.0112 ± 0.0002	0.0206 ± 0.0006	0.011 ± 0.0005	$p = 0.085$	$p < 0.001$	Tukey

Data are expressed as mean ± standard error

CTP CT perfusion, *BV* blood volume, *BF* blood flow, *CL* clearance rate, *MVD* microvessel density

* All $p < 0.05$ in the Games–Hotwell multiple comparison test

† All $p < 0.001$ in the Tukey multiple comparison test

process and accurately depicted the hemodynamic changes evaluated by volume CTP during a gouty attack. Angiogenesis develops very early in the advanced stage of gouty attack, and reduction of vascular permeability goes rapidly during resolution of gouty attack. Additionally, this CTP rabbit model affords an ideal platform for further study of the relationship between vascular reaction and inflammatory cells or chemical mediators in gouty arthritis, and also helps to find a new therapeutic target to prevent a gout attack.

Funding This study has received funding from The science and technology development of Shandong province (2011GSF11834).

Compliance with ethical standards

Guarantor The scientific guarantor of this publication is Qing Yang.

Conflict of interest The authors declare that they have no competing interests.

Statistics and biometry No complex statistical methods were necessary for this paper.

Informed consent Approval from the institutional animal care committee was obtained.

Ethical approval Institutional Review Board approval was obtained.

Methodology
- Prospective
- Randomized controlled trial/experimental
- Performed at one institution

References

1. Martinon F (2010) Mechanisms of uric acid crystal-mediated autoinflammation. Immunol Rev 233:218–232
2. Chhana A, Lee G, Dalbeth N (2015) Factors influencing the crystallization of monosodium urate: a systematic literature review. BMC Musculoskelet Disord 16:296
3. Landis RC, Yagnik DR, Florey O et al (2002) Safe disposal of inflammatory monosodium urate monohydrate crystals by differentiated macrophages. Arthritis Rheum 46:3026–3033
4. Henrotin Y, Pesesse L, Lambert C (2014) Targeting the synovial angiogenesis as a novel treatment approach to osteoarthritis. Ther Adv Musculoskelet Dis 6:20–34
5. Bevilacqua A, Barone D, Malavasi S, Gavelli G (2014) Quantitative assessment of effects of motion compensation for liver and lung tumors in CT perfusion. Acad Radiol 21:1416–1426
6. Cros M, Geleijns J, Joemai RM, Salvadó M (2016) Perfusion CT of the brain and liver and of lung tumors: use of Monte Carlo simulation for patient dose estimation for examinations with a cone-beam 320-MDCT scanner. AJR Am J Roentgenol 206:129–135
7. Scanu A, Oliviero F, Gruaz L et al (2010) High-density lipoproteins downregulate CCL2 production in human fibroblast-like synoviocytes stimulated by urate crystals. Arthritis Res Ther 12: R23
8. Phelps P, McCarty DJ Jr (1966) Crystal-induced inflammation in canine joints. II. Importance of polymorphonuclear leukocytes. J Exp Med 124:115–126
9. Coderre TJ, Wall PD (1987) Ankle joint urate arthritis (AJUA) in rats: an alternative animal model of arthritis to that produced by Freund's adjuvant. Pain 28:379–393
10. Nishimura A, Akahoshi T, Takahashi M et al (1997) Attenuation of monosodium urate crystal-induced arthritis in rabbits by a neutralizing antibody against interleukin-8. J Leukoc Biol 62:444–449
11. Pineda C, Fuentes-Gómez AJ, Hernández-Díaz C et al (2015) Animal model of acute gout reproduces the inflammatory and ultrasonographic joint changes of human gout. Arthritis Res Ther 17: 37
12. Meijerink MR, van Waesberghe JH, van Schaik C et al (2010) Perfusion CT and US of colorectal cancer liver metastases: a correlative study of two dynamic imaging modalities. Ultrasound Med Biol 36:1626–1636
13. Steiger S, Harper JL (2014) Mechanisms of spontaneous resolution of acute gouty inflammation. Curr Rheumatol Rep 16:392
14. Steiger S, Harper JL (2013) Neutrophil cannibalism triggers transforming growth factor β1 production and self regulation of neutrophil inflammatory function in monosodium urate monohydrate crystal-induced inflammation in mice. Arthritis Rheum 65:815–823
15. Martinon F, Pétrilli V, Mayor A, Tardivel A, Tschopp J (2006) Gout-associated uric acid crystals activate the NALP3 inflammasome. Nature 440:237–241
16. Fuchs TA, Abed U, Goosmann C et al (2007) Novel cell death program leads to neutrophil extracellular traps. J Cell Biol 176: 231–241
17. Kumar V, Abbas AK, Aster JC (2018) Robbins Basic Pathology, 10th edn. Elsevier, Pennsylvania Philadelphia